Journal of Thermal Analysis and Calorimetry, Vol. 78 (2004) 639–655

ATMOSPHERIC EFFECT FOR THERMAL PROCESS OF INDIUM HYDROXOFORMATE

T. Arii[1*], *A. Kishi*[2] *and Y. Sawada*[3]

[1]Thermal Analysis Division, Rigaku Corporation, 3-9-12 Matsubara, Akishima, Tokyo 196-8666, Japan
[2]X-ray Application Center, Rigaku Corporation, 3-9-12 Matsubara, Akishima, Tokyo 196-8666, Japan
[3]Department of Applied Chemistry, Faculty of Engineering, Tokyo Institute of Polytechnics, 1583 Iiyama, Atsugi, Kanagawa 243-0297, Japan

Abstract

The influence of thermal process for indium hydroxoformate, $In(OH)(HCO_2)_2$, used as one of the precursor material of ITO transparent conducting films, has been successfully investigated in some controlled atmospheres by unique thermal analyses equipped with a humidity generator, which are thermogravimetry – differential thermal analysis (TG-DTA), thermogravimetry in conjunction with evolved gas analysis using mass spectrometry (TG-MS) and simultaneous measurement of differential scanning calorimetry and X-ray diffractometry (XRD-DSC). The thermal process in dry gas atmosphere by linear heating experiment was indicated through a single-step reaction between 200 and 300°C, while the thermal process in the atmosphere of controlled humidity proceeded through two-step reactions and the formation of crystalline indium oxide (In_2O_3) was effectively promoted and completed at the lower temperatures with introducing water vapor in the atmosphere. The thermal process changed dramatically by introducing water vapor and was quite different from that in dry gas atmosphere. Pure In_2O_3 was synthesized in inert atmosphere of controlled humidity and could be easily formed at temperatures below 260°C. The XRD-DSC equipped with a humidity generator revealed directly the crystalline change from $In(OH)(HCO_2)_2$ to In_2O_3 and the formation of the intermediate during the thermal decomposition. A detailed thermal process of $In(OH)(HCO_2)_2$ and the effect of heating atmosphere are discussed.

Keywords: atmosphere of controlled humidity, In_2O_3, $In(OH)(HCO_2)_2$, TG-MS, thermal process, XRD-DSC

Introduction

Tin-doped In_2O_3 (indium-tin-oxide) transparent conducting films are widely used as electrodes of liquid crystal displays, solar cells, heat reflecting windows, *etc*. [1]. These ITO films have been mainly manufactured by physical vapor deposition (PVD) such as the magnetron sputtering process so that many investigations have focused on the films

* Author for correspondence: E-mail: t-arii@rigaku.co.jp

1388–6150/2004/ $ 20.00

Akadémiai Kiadó, Budapest
Kluwer Academic Publishers, Dordrecht

deposited by the PVD process. On the other hand, the dip-coating process has been known as one of the chemical methods of producing ceramics thin films; a substrate, for example a glass plate, is dipped into the solution containing an organic precursor of the ceramics material, raised slowly to evaporate the solvent, and then heated to form the oxide film. Generally, the film qualities such as transparency and resistivity of ITO film prepared by dip-coating method do not satisfy compared with those of PVD and relatively high temperature is need for the calcination process, although this chemical process is advantageous for cost-saving mass-production of large-area thin films with uniform thickness. In addition, the thermal process (decomposition, oxidation, etc.) is particularly important to control the structure and properties of ITO films, because these reactions are strongly influenced by the experimental conditions such as heating atmospheres [2, 3]. For instance, because ITO film for liquid crystal is deposited on the resin film such as polyimide color filter, it is desirable that the substrate temperature during the film fabrication process is controlled below 220°C. Therefore, low temperature synthesis via sol-gel process and/or thermal decomposition of metal-organic precursors has attracted attention in the fields. Although the thermal treatment has been recognized as one of the important processes in many ceramics fabrication, fundamental studies are scarce and many cases are achieved empirically. The basic data are thought to be useful for the design of optimum fabrication control, and to clarify the mechanism of thermal process.

Indium carboxylates have been studied as the precursor materials for ITO films using dip-coating method [4–6]. It is therefore of interest to study the possibility of low temperature synthesis using indium carboxylates, and decomposition to form In_2O_3. Several studies of the thermal decomposition of metal-organic compounds have been reported in [7–9]. Recently, the present authors focused on the effect of heating atmosphere for the thermal process of metal carboxylates using novel thermal analyses [10–12]: sample-controlled thermal analysis (SCTA), simultaneous coupling measurement of thermogravimetric – differential thermal analysis and mass spectrometry (TG-DTA-MS) [13–16], and simultaneous measurement of X-ray diffractometry – differential scanning calorimetry (XRD-DSC) [17–19]. To elucidate the underlying thermal process in detail such complementary thermal methodologies based upon hyphenated technology, satisfactorily improved the data interpretation.

The aim of this paper is to analyze the thermal processes of $In(OH)(HCO_2)_2$ in inert and oxidative atmospheres of controlled humidity, and especially to investigate the affect of water vapor on the change of reaction mechanism and formation temperature of In_2O_3. The thermal behaviors of $In(OH)(HCO_2)_2$ under such different atmospheric conditions were investigated by means of TG-DTA, TG-DTA-MS and XRD-DSC. The thermal pathway was remarkably influenced by changing the atmosphere and is discussed.

Experimental

Specimen

The In_2O_3 powders (20 g, purity 5N, particle size <1 μm, Kojyundo Chemical Laboratories, Inc.) were refluxed in excess amount of formic acid (500 mL, 99%, Wako Pure Chemical, Inc.) for 2 weeks. The solution was heated at 60°C in vacuo (0.3 atm) for 3 h to evaporate formic acid and water to obtain white powders of indium hydroxoformate. An X-ray diffraction spectrum corresponding to the postulated composition of crystalline $In(OH)(HCO_2)_2$ was shown in Fig. 1. The diffraction of unreacted In_2O_3 [20] was not detected.

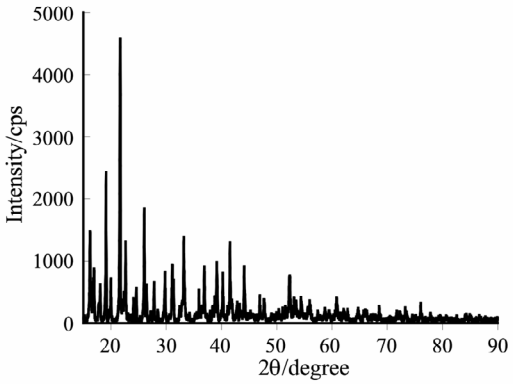

Fig. 1 XRD diagram of indium hydroxoformate, $In(OH)(HCO_2)_2$

Apparatus

Thermogravimetric-differential thermal analysis, TG-DTA, was performed using a Rigaku Thermo Plus 8120D system. The specimen mass of ca. 5 mg were weighed into an aluminum crucible, and were heated up to 450°C in dry air, high-purity dry helium (99.99%) or nitrogen (99.99%), simulated air (mixture gas of 20% oxygen in helium balance) and their atmospheres of controlled humidity, with a flow rate of 200 mL min^{-1}.

The spectra of the gaseous products evolved from the specimen in TG-DTA are simultaneously monitored with a quadrupole mass spectrometer (Model QP-5050A, Shimadzu). This mass spectrometer (MS) is connected to TG-DTA via a gas transfer tube with 3000 mm long stainless capillary of an internal diameter of 0.5 mm, whose the capillary internal surface is inactivated. Details of the TG-DTA-MS equipment are described elsewhere [21, 22]. All of the transfer pathway was kept at 280°C to minimize condensation of the gaseous products evolved from the specimen. The acceleration voltage of the ionization for MS was fixed at potential of 70 eV. Detection mass region of m/z was fixed at 10–350. In a series of the simultaneous TG-DTA-MS experiments, to ignore desorption of any components adsorbed in the reference material such as α-Al_2O_3, only an empty crucible was used as reference.

The crystal structures of the specimens quenched from TG-DTA experiments were confirmed by X-ray diffractometer (XRD; Model RINT2200V/PC, Rigaku) using graphite-monochromated CuK_α radiation (λ=1.5405 Å). A line shape X-ray source was operated at 50 kV and 40 mA and the data were collected in the range of 2θ=2 to 90° with an interval of 0.02° and a scan speed of 0.5° min^{-1}.

The simultaneous measuring apparatus for XRD-DSC consisted of a specific heat-flux type of DSC (Model Thermo Plus DSC8320, Rigaku) modified and combined with an X-ray diffractometer (XRD; Model RINT-Ultima$^+$, Rigaku). Details of the XRD-DSC apparatus are described elsewhere [23]. The XRD-DSC measurements were carried out from ambient temperature to 280°C at a heating rate of 3°C min^{-1}. The specimen was mounted on a square aluminum container (7×7 mm and 0.25 mm in depth). A line shape X-ray source was operated at 50 kV and 40 mA and the data were collected in the range of $10°<2\theta<42°$ with an interval of 0.02° and a scan speed of 20° min^{-1}. With a temperature scan rate of 3°C min^{-1}, the change of sample temperature during each XRD scan corresponds to approx. 5°C, i.e. the XRD diagram obtained during each XRD scan expresses the mean spectrum of the temperature range of every 5°C. The θ and 2θ calibration was done using a silicon standard.

The special type of TG-DTA equipped with an electrical furnace surrounded by a specially designed water-jacket instead of conventional type of furnace was used in order to prevent condensation of water vapor. The isothermally controlled water into the water-jacket was supplied by a heating circulator (Model F25-MV, Julabo Labortechnik Gmbh, Seelbach, Germany). This modified type of TG-DTA apparatus was coupled with a humidity generator (Model HUM-1, Rigaku). The integrated humidity-controlled TG-DTA system is described elsewhere [12]. The mass-flow controllers in the humidity generator are used to control automatically the flow rate of dry nitrogen gas, so that the humidity/temperature sensor located into the gas injection port of the furnace protection tube indicates target constant pre-selected values. This humidity generator can provide wet gases in the humidity range from 25°C–5%RH to 60°C–90%RH. Additionally, the present humidity generator was also easily coupled with the XRD-DSC apparatus.

Temperature calibration of TG-DTA and DSC was performed using pure metals of In, Sn and Pb.

Results and discussion

TG-DTA in dry gas atmosphere

The typical TG-DTA curves for $In(OH)(HCO_2)_2$ at a heating rate of 10°C min^{-1} in dry helium flow are shown in Fig. 2. The thermal process exhibited a single-reaction step accompanying a discernible shoulder in course of DTA peak; the total mass loss of 45.5% up to 300°C was accompanied by an endothermic DTA peak at 270°C. The mass loss did not agree with the theoretical one corresponding to the formation of indium oxide (In_2O_3). The theoretical mass losses corresponding to the formations of In_2O_3 and metallic indium were also represented in Fig. 2 as reference. The mass loss

was situated between the theoretical formation of In_2O_3 and metallic indium so that the residue was presumed to be a mixture of In_2O_3 and metallic indium. In order to clarify the existence of metallic indium in the residue, the specimen quenched from TG-DTA at 450°C was re-heated in helium atmosphere. The results of this second run TG-DTA are also shown in Fig. 2 as dotted line. Although no mass loss was observed during the thermal analysis, only a sharp endothermic DTA peak was clearly observed around 160°C. The endothermic phenomenon can be interpreted as the fusion of residual metallic indium, because an extrapolated onset-temperature of DTA peak (156°C) agreed satisfactorily with melting point of metallic indium. The facts supported that the total mass loss was higher than theoretical mass loss corresponding to the formation of In_2O_3.

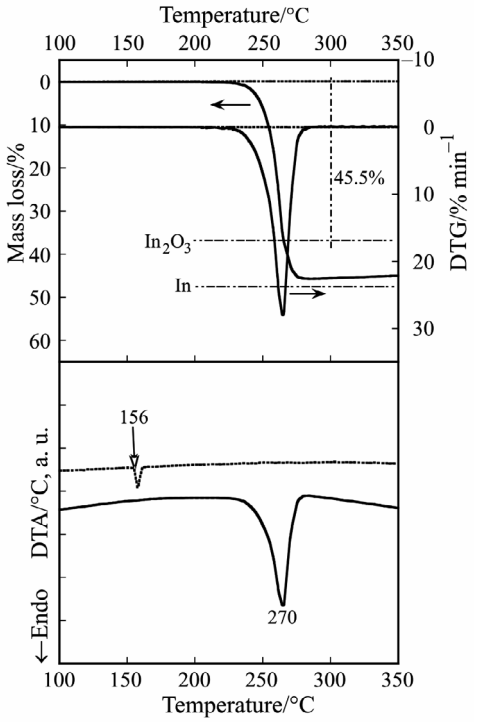

Fig. 2 Typical TG-DTA curves for $In(OH)(HCO_2)_2$ at 10°C min^{-1} in dry helium flow

The typical TG-DTA curves for $In(OH)(HCO_2)_2$ at a heating rate of 10°C min^{-1} in dry simulated air flow (20% oxygen in helium atmosphere) are shown in Fig. 3. The thermal change was basically identical with that in helium atmosphere except an exothermic mass loss observed remarkably at ~300°C. The total mass loss of 40.1% up to 300°C was accompanied by an exothermic DTA peak at 290°C. The theoretical mass losses corresponding to the formations of In_2O_3 and metallic indium were also represented in Fig. 3 as reference. Although the total mass loss was lower than that in helium atmosphere, the

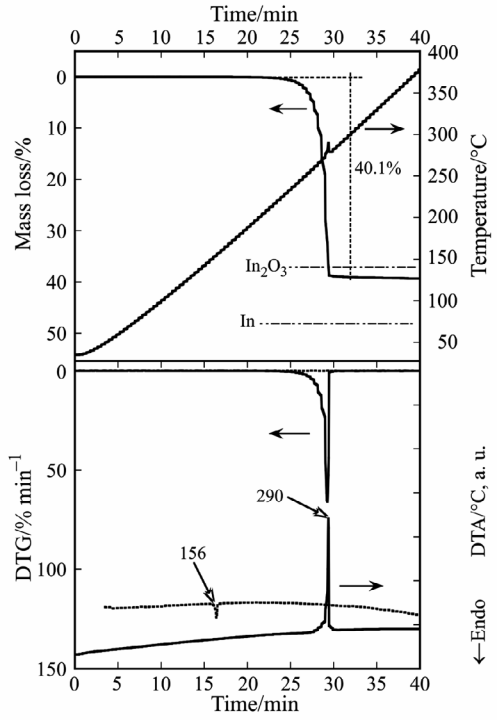

Fig. 3 Typical TG-DTA curves for $In(OH)(HCO_2)_2$ at 10°C min^{-1} in dry simulated air flow

mass loss obtained was still situated between the theoretical mass losses corresponding to the formation of In_2O_3 and metallic indium so that the residual composition was presumed to be a mixture of In_2O_3 and metallic indium. However, the mass loss was smaller than that in dry helium atmosphere, suggesting the acceleration of oxidation to In_2O_3. The results of second run TG-DTA in helium atmosphere for the quenched specimen from TG-DTA at 450°C in simulated air atmosphere are also shown in Fig. 3 as dotted line. Only a sharp endothermic DTA peak appeared clearly around 160°C, and an extrapolated onset-temperature (156°C) of DTA peak agreed well with melting point of metallic indium. The results suggested that the residue after the thermal analysis in simulated air atmosphere is to be a mixture of In_2O_3 and metallic indium.

TG-DTA in controlled-humidity atmosphere

The typical TG-DTA curves for $In(OH)(HCO_2)_2$ at a heating rate of 10°C min^{-1} in the simulated air atmosphere of controlled humidity (P_{H_2O} = 60°C 60%RH) are shown in Fig. 4. The thermal change was basically identical with that in dry simulated air atmosphere, except a broad endothermic mass loss observed followed by a sharp exothermic mass loss at ~270°C. The mass loss of 39.1% up to 300°C was slightly lower than that in dry simulated air atmosphere and was initiated from the lower tempera-

tures. The thermal decomposition seemed to be complicated by the overlapping of the endothermic and exothermic phenomena. The theoretical mass losses corresponding to the formation of In_2O_3 and metallic indium were also represented in Fig. 4 as reference. The mass loss obtained was still situated between the theoretical mass losses corresponding to the formations of In_2O_3 and metallic indium so that the residue was presumed to be a mixture of In_2O_3 and a small amount of metallic indium. The mass loss decreased by introducing humidity, suggesting the acceleration of oxidation to In_2O_3. The results of the second run TG-DTA in dry helium atmosphere for the quenched specimen from TG-DTA at 450°C in the simulated air atmosphere of controlled humidity are also shown in Fig. 4. A sharp endothermic DTA peak with an extrapolated onset-temperature (156°C) corresponding to melting point of metallic indium can be slightly detected. The results suggested that the residue after the thermal analysis in the simulated air atmosphere of controlled humidity is to be a mixture of In_2O_3 and the small amount of metallic indium.

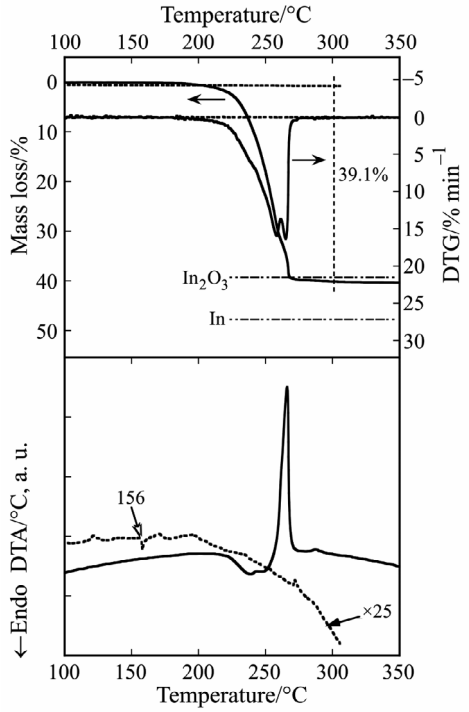

Fig. 4 Typical TG-DTA curves for $In(OH)(HCO_2)_2$ at 10°C min^{-1} in simulated air atmosphere of controlled humidity (P_{H_2O}= 60°C 60%RH)

The typical TG-DTA curves for $In(OH)(HCO_2)_2$ at a heating rate of 10°C min^{-1} in nitrogen atmosphere of controlled humidity (P_{H_2O} = 60°C 60%RH) are shown in Fig. 5. The thermal process exhibited two-step reactions accompanying double endo-

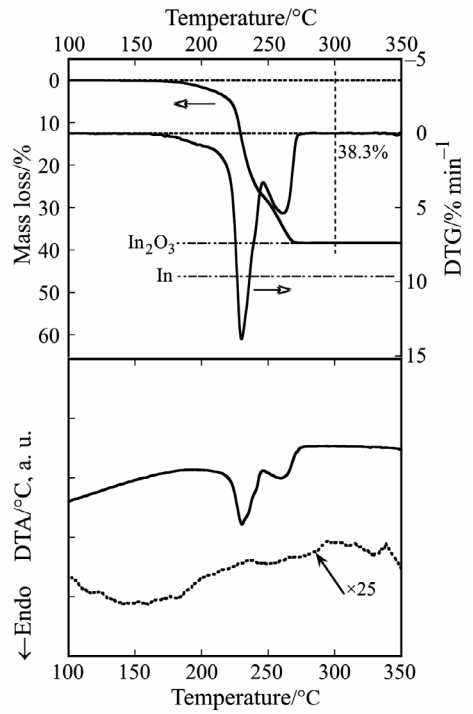

Fig. 5 Typical TG-DTA curves for $In(OH)(HCO_2)_2$ at 10°C min^{-1} in nitrogen atmosphere of controlled humidity (P_{H_2O}= 60°C 60%RH)

thermic DTA peaks and was initiated from the lower temperatures than that in the dry nitrogen atmosphere. The mass loss of 38.3% up to 300°C agreed satisfactorily with the theoretical one corresponding to the formation of In_2O_3 so that the residue was presumed to be only In_2O_3. No endothermic peak in the second run TG-DTA was observed in the specimen quenched from TG-DTA at 450°C in nitrogen atmosphere of controlled humidity, supporting without the residual metallic indium. In the present experimental atmospheres, it suggested that pure In_2O_3 powder is only synthesized in nitrogen atmosphere of controlled humidity.

However, it cannot say that above mentioned interpretations are enough to explain In_2O_3 formed during the thermal analysis.

XRD analysis

In order to elucidate the thermal decomposition process changed by atmospheric difference and support the results of TG-DTA, it is important to identify the residual solid substances formed from TG-DTA. Figure 6 shows a comparison of the XRD diagrams for the specimens quenched from 450°C in the various heating atmospheres using TG-DTA at 5°C min^{-1}. The thermal decomposition product obtained from TG-DTA in dry nitrogen atmosphere was clearly identified as a mixture of crystalline

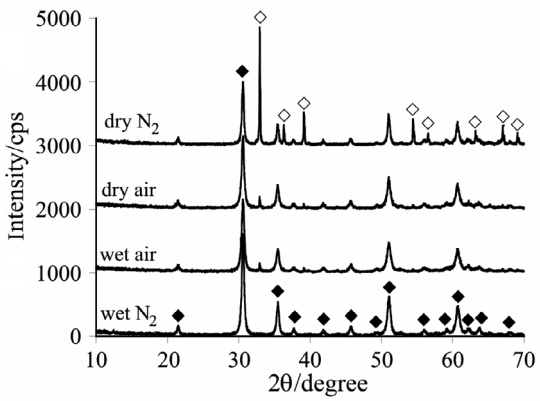

Fig. 6 Comparison of XRD diagrams for the quenched specimens from TG-DTA at 450°C in various heating atmospheres. ◇ – In, ◆ – In_2O_3

In_2O_3 and metallic indium, from its XRD pattern search. On the other hand, the similarity of the XRD spectra between the specimens quenched from TG-DTA in dry air and air atmosphere of controlled humidity is evident, except for the small difference of XRD intensity. Both are dominant by the spectra consisted of crystalline In_2O_3 and metallic indium. By introducing the water vapor into dry air atmosphere, the intensity of the XRD spectra corresponding to metallic indium decreased with accelerating oxidation of the specimens. Moreover, the XRD spectrum for the specimen heat-treated in nitrogen atmosphere of controlled humidity showed only crystalline In_2O_3 without the spectrum of metallic indium. Therefore, these findings supported the results of TG-DTA that pure In_2O_3 powder can be synthesized only in nitrogen atmosphere of controlled humidity.

TG-MS analysis

Figure 7a shows the typical results of TG-MS for $In(OH)(HCO_2)_2$ in helium atmosphere at a heating rate of 10°C min^{-1}, where the total ion current (TIC) indicates sum of the ion current for all detected species. Figure 7b illustrates the mass spectrum of the gases detected at the TIC peak of 270°C, where the mass spectrum indicate the relative ion intensities after subtracting the background spectrum before heating. The TIC curve synchronized completely with the derivative TG (DTG) curve, suggesting that time lag of the interface between TG-DTA and MS is negligible. By comparing with the mass spectra registered in NIST-MS database, the mass loss was mainly assigned to the evolutions of carbon dioxide (*m*/*z* 12, 28 and 44), water vapor (*m*/*z* 17 and 18) and formic acid (*m*/*z* 17, 29, 45 and 46), respectively, suggesting the thermal decomposition of the specimen. Furthermore, a small amount of formaldehyde (*m*/*z* 28, 29 and 30) was presumably ascribed because the relative ion intensities of *m*/*z* 29 and 30 were slightly stronger than those of the fragmentations of formic acid registered in NIST-MS database. Figure 8 exhibits the molecular ion chromatograms of *m*/*z* 18, 29, 44 and 46 characterized the above identified species as a function of

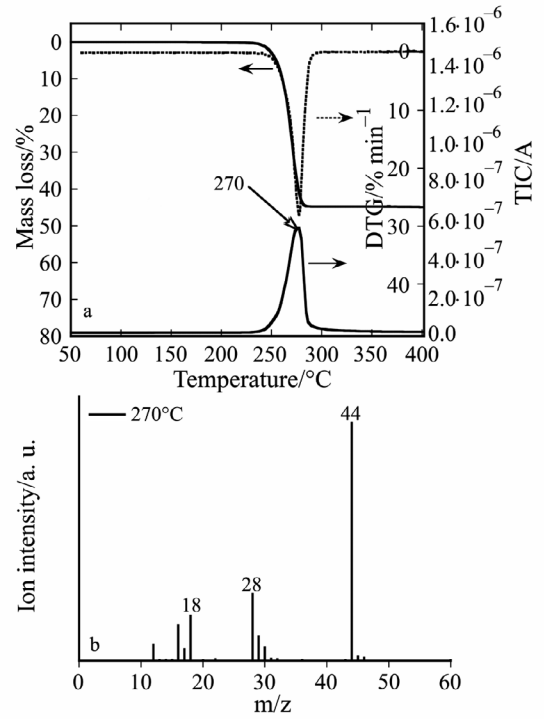

Fig. 7 TG-MS results of $In(OH)(HCO_2)_2$ at 10°C min^{-1} in dry helium flow.
a – TG, DTG and TIC curves, b – Mass spectrum of the TIC peak at 260°C

the temperature, together with the TG-DTA curves. Evolution of water vapor and carbon dioxide, formic acid and formaldehyde occurred concurrently by the single decomposition step, since these detected ions synchronized completely to each other.

The above in mind, tentative following decomposition schemes in dry inert atmosphere are proposed assuming that metallic indium and In_2O_3 are separately formed, respectively.

$$2In(OH)(HCO_2)_2 \rightarrow 2In+2H_2O+HCOOH+3CO_2 \quad (1)$$

$$2In(OH)(HCO_2)_2 \rightarrow In_2O_3+HCOH+2HCOOH+CO_2 \quad (2)$$

These parallel reactions were competitively occurred to each other, since the residue after the thermal analysis in dry inert atmosphere was identified as a mixture of In_2O_3 and metallic indium. Also, the total mass loss may be strongly influenced by the experimental conditions such as heating rate, sample mass and flow rate of atmosphere.

Figure 9a shows the typical results of TG-MS for $In(OH)(HCO_2)_2$ in dry simulate air atmosphere at a heating rate of 10°C min^{-1}. The TIC indicates sum of the ion current for all detected species after subtracting the background spectrum including oxygen (*m*/*z* 16, 32) saturated in the atmosphere before heating. Figure 9b illustrates the ion chromatograms (MC) extracted from the mass spectrum at TIC peak

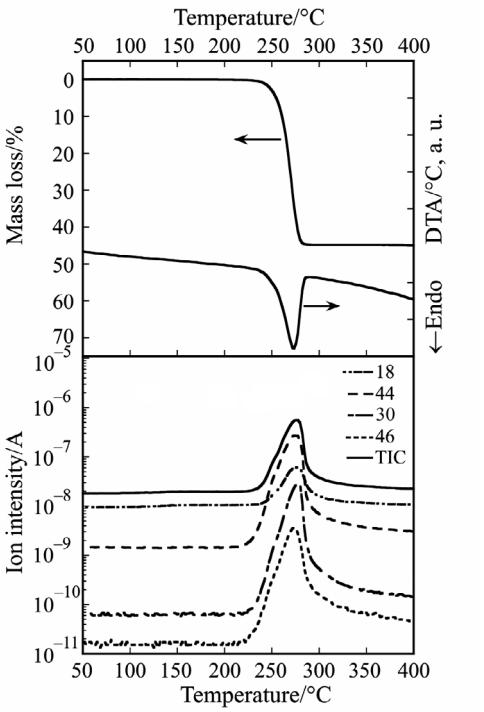

Fig. 8 TG-DTA curves in dry helium flow and ion chromatograms of molecular ions (*m*/*z* 18, 30, 44 and 46) for evolved gases.
m/*z* 18, H_2O; *m*/*z* 30, CH_2O; *m*/*z* 44, CO_2; CH_2O_2; *m*/*z* 46

of 270°C. The MC and DTG curves synchronized completely to each other. The exothermic mass loss was interpreted as combustion of the evolved formic acid and formaldehyde; the simultaneous evolution of carbon dioxide and water vapor supported this hypothesis. The rapid mass loss accompanying a rapid evolution of formic acid and carbon dioxide was understood to be the rapid decomposition accelerated by the combustion heat indicated as the remarkable temperature increase in Fig. 9a. It can be interpreted that metallic indium in the residue after thermal analysis was formed during the incomplete combustion for the specimen caused by this rapid temperature increase.

Figure 10 shows the typical results of TG-MS for $In(OH)(HCO_2)_2$ in helium atmosphere of controlled humidity (P_{H_2O} = 60°C 60%RH) at a heating rate of 10°C min^{-1}. The thermal process seems to proceed through two-step endothermic mass losses accompanying double gas evolution peaks. The mass loss up to 300°C agreed satisfactorily with the theoretical one corresponding to the formation of In_2O_3. The first step mass loss at the inflection point resolved from the maximum between the DTG peaks is 27.0% at 245°C. Thus, the other mass loss for the second step corresponds to 11.3% up to final point of 300°C. Consequently, we deduce from these mass losses that an intermediate product was formed in the course of decomposition process. Figure 11 illus-

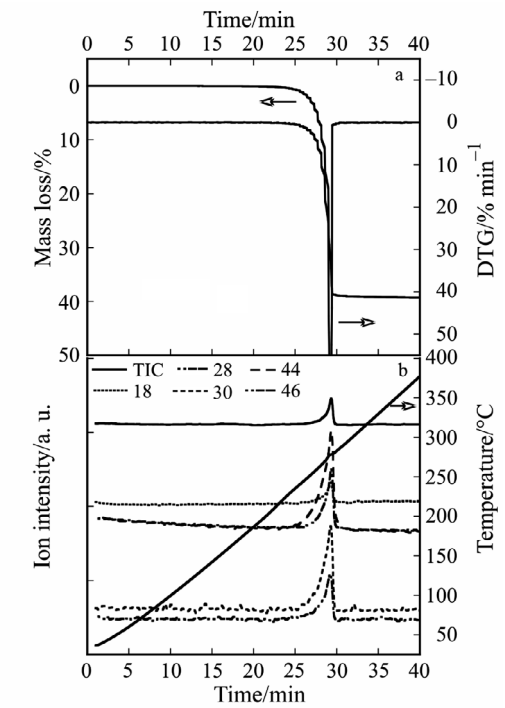

Fig. 9 TG-MS results of $In(OH)(HCO_2)_2$ at 10°C min^{-1} in dry simulated air flow. a – TG, DTA and TIC curves, b – ion chromatograms extracted from mass spectrum of evolution gas peak of TIC at 270°C.
m/*z* 18, H_2O; *m*/*z* 30, CH_2O; *m*/*z* 44, CO_2; CH_2O_2; *m*/*z* 46

trates the mass spectra for the evolution gases detected at the TIC peaks of 235 and 260°C, respectively. We can learn that the both mass spectra were quite different to each other, suggesting the different gas components were formed during each stage. By comparing with the mass spectra of NIST-MS database, the first mass loss of 27.0% was mainly assigned to the evolutions of carbon dioxide and formic acid, respectively. Also, the second mass loss of 11.3% was assigned to the evolution of carbon dioxide and very small amount of formic acid.

From these findings, the formation of the intermediate was speculated by allowing $In(OH)(HCO_2)_2$ to react with water vapor according to the reaction

$$2In(OH)(HCO_2)_2+H_2O\rightarrow In_2(OH)_3(HCO_2)+2HCOOH+CO_2 \quad (3)$$

The intermediate product $In_2(OH)_3(HCO_2)$ was decomposed by the following subsequent reaction if HCOOH is negligible.

$$In_2(OH)_3(HCO_2)\rightarrow In_2O_3+2H_2+CO_2 \quad (4)$$

Here, H_2 represents the unidentified gaseous products. The mass losses for estimated from the first and second stages agreed satisfactorily with those of the theoreti-

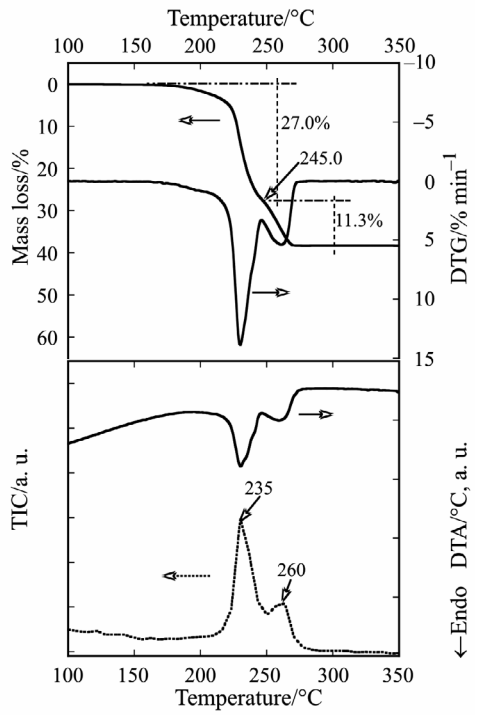

Fig. 10 TG-MS results of $In(OH)(HCO_2)_2$ at 10°C min^{-1} in helium atmosphere of controlled humidity (P_{H_2O}= 60°C 60%RH)

cal mass losses presuming to Eqs (3) and (4) which are 26.6 and 10.8%, respectively. Finally, pure In_2O_3 could be only easily synthesized in the condition of inert atmosphere of controlled humidity.

XRD-DSC analysis

In order to analyze in detail the thermal process for the formation of crystalline In_2O_3 formed in inert atmosphere of controlled humidity, it is important to observe the formation products changed during the solid phase. The XRD-DSC for $In(OH)(HCO_2)_2$ at 3°C min^{-1} in nitrogen atmosphere of controlled humidity (P_{H_2O} = 60°C 60%RH) is shown in Fig. 12; the relationship between the XRD patterns and the DSC curve can be clearly observed in this figure. The XRD patterns corresponding to each point on DSC curve with the same temperature range are represented on the left side. The change of diffraction intensities in the XRD patterns appeared clearly corresponding to the DSC curve. The DSC curve indicates that the thermal process of the specimen begins at around 200 and ends at 260°C. The shape of the DSC curve corresponds approximately with that of the DTA in Fig. 8, except for the reaction temperature. The difference should be attributed to the heating rate: 10 and 3°C min^{-1}. The DSC curve showed a relatively sharp peak around 210°C followed by a broad peak, and sug-

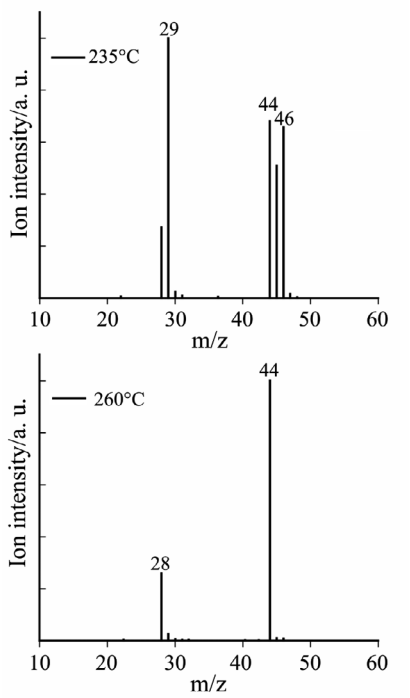

Fig. 11 Mass spectra for evolution gas peaks of TIC at 235 and 260°C

gested that the thermal process consists of multiple-step reactions including the formation of an intermediate. Similarly, it can be clearly observed that the change in XRD patterns gradually starts from around 200°C, and completes after the second broad DSC peak at 250°C. It seems likely, moreover, that an existence of different solid phases during the thermal process is revealed by changing the XRD patterns. As discussed below, the XRD data recorded simultaneously with DSC scan give us very important information in regard to the assurance of the existence of the intermediate compound formed during the endothermic reaction.

The XRD patterns obtained after the endothermic decomposition have sharp crystalline peaks, indicating pure crystalline products. The XRD profiles of the resulting products observed after the endothermic DSC peak agreed satisfactorily with that of In_2O_3. Here, the characteristic diffraction peaks around 18.5, 24.2 and 40° in the XRD profile disappeared completely after the first endothermic DSC peak (around 215°C), suggesting the structural phase change such as the formation of new intermediate compound.

The DSC curve and the integrated XRD intensity in the range of the diffraction angles characterizing the above structural changes are compared in Fig. 13 as a function of temperature. The integrated XRD intensity curves for the diffraction angles of 15.8–16.5 and 18.5–19.5° related to crystalline $In(OH)(HCO_2)_2$ show broad sigmoidal decays corresponding to the progress of the decomposition, while an incre-

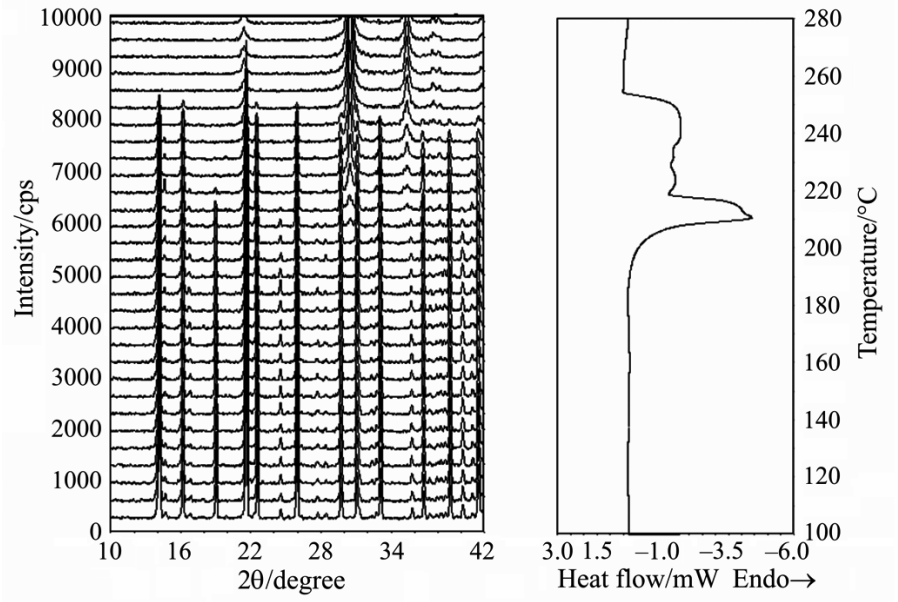

Fig. 12 Relationship between DSC curve and XRD patterns in thermal process of $In(OH)(HCO_2)_2$ by XRD-DSC at 3°C min^{-1} in nitrogen atmosphere of controlled humidity (P_{H_2O}= 60°C 60%RH)

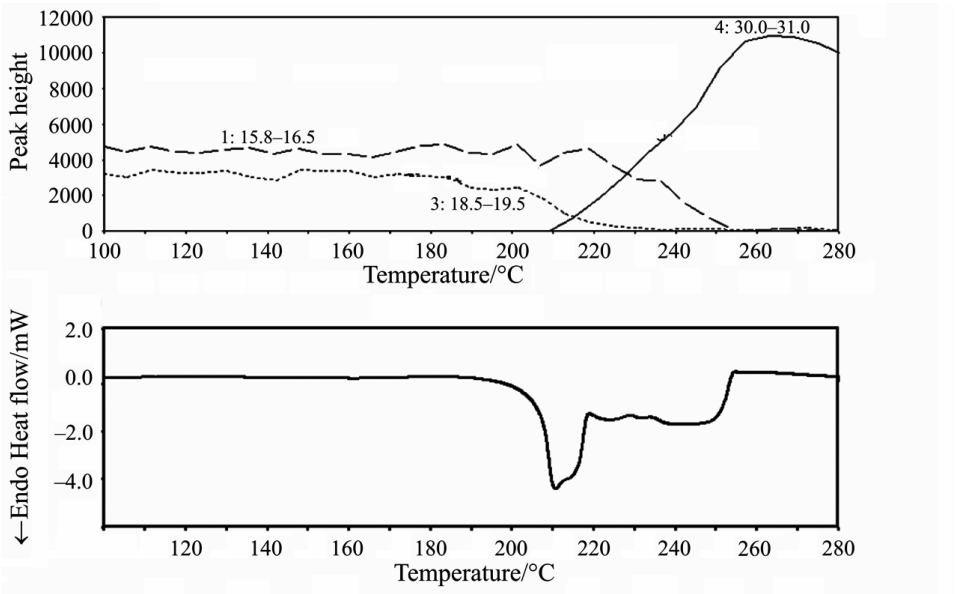

Fig. 13 Integrated intensity change of XRD peaks *vs*. temperature (upper) and DSC curve (lower) in nitrogen atmosphere of controlled humidity.
Curve 1 – diffraction angle 15.8–16.5°, Curve 2 – 18.5–19.5°, Curve 3 – 30–31°C

ment of the integrated peak intensity in the diffraction angles of 30–31° reveals a concurrent growth of crystalline In_2O_3. The XRD intensity curve integrated from the diffraction angle range of 18.5–19.5° disappears completely after the first sharp DSC peak and is obviously earlier than that integrated from the diffraction angle range of 15.8–16.5°. Consequently, it is concluded that the crystalline $In(OH)(HCO_2)_2$ was directly decomposed to crystalline In_2O_3 by reacting with the water vapor introduced into the atmosphere and that the intermediate compound was concurrently formed in course of the decomposition. Furthermore, pure crystalline In_2O_3 was easily synthesized at lower temperature region below 260°C.

Conclusions

Thermal processes of $In(OH)(HCO_2)_2$ in inert and oxidative atmospheres, their atmospheres of controlled humidity were investigated by TG-DTA-MS and XRD-DSC equipped with a humidity generator. Thermal processes in both dry inert and oxidative atmospheres were indicated through a single-step decomposition at ~300°C accompanying the evolution of carbon dioxide, water vapor, formaldehyde and formic acid, respectively. Because the mass losses were situated between the theoretical ones corresponding to the formation of In_2O_3 and metallic indium, the residue after the thermal analysis was presumed to be a mixture of In_2O_3 and metallic indium. On the other hand, the thermal process of $In(OH)(HCO_2)_2$ was remarkably influenced by the water vapor introduced in the atmospheres, and was quite different from that in dry gas atmosphere. With introducing of water vapor, the formation of In_2O_3 was accelerated, and contrary to this, the formation of metallic indium was effectively inhibited. Particularly, the thermal process in inert atmosphere of controlled humidity proceeded through two-step endothermic decomposition accompanying double gas evolution peaks and the mass loss agreed satisfactorily with the theoretical one corresponding to the formation of In_2O_3. The existence of the intermediate, $In_2(OH)_3(HCO_2)$, was tentatively speculated by allowing $In(OH)(HCO_2)_2$ to react with water vapor.

The XRD-DSC in nitrogen atmosphere of controlled humidity revealed that $In(OH)(HCO_2)_2$ was directly decomposed to crystalline In_2O_3 by reacting with water vapor, and the intermediate compound was concurrently formed in course of the thermal decomposition.

These results demonstrated that unique thermal analyses such as TG-DTA-MS and XRD-DSC equipped with a humidity generator are indispensable tools for determining the decomposition mechanism in sufficient detail to understand complicated thermal processes during syntheses of advanced ceramic materials. Especially, the synthesis of metal oxides via thermal decomposition of metal-organic precursors by using the atmosphere of controlled humidity will become effective in various fields as a kind of low temperature synthesis.

References

1 Y. Shigesato and I. Yasui, Oyo Bunseki, 64 (1995) 1225.

2 F. Yamaguchi, Abstract for the 9th Symposium, the Materials Research Society of Japan, Kawasaki, Japan 1997, p. 113.
3 F. Yamaguchi, Master Thesis, Tokyo Institute of Polytechnics, 1998, pp. 19–73.
4 Y. Sawada, T. Shigaraki, S. Seki, M. Ogawa, T. Senda, T. Nishide and J. Matsushita, J. Mass Spectrom. Soc. Jpn., 46 (1998) 292.
5 S. Seki, T. Suzuki, T. Senda, T. Nishide and Y. Sawada, Thermochim. Acta, 352–353 (2000) 75.
6 K. Shimizu, M. Yamamoto, S. Seki, T. Arii, M. Ogawa and Y. Sawada, Materials Integration, 14 (2001) 55.
7 K. Manabe and M. Ogawa, Nihonkagakukaishi, 7 (1983) 1092.
8 I. Mayer and F. Kassierer, J. Inorg. Nucl. Chem., 28 (1966) 2430.
9 D. A. Edwards and R. N. Hayward, Can. J. Chem., 46 (1968) 3343.
10 T. Arii, A. Kishi, M. Ogawa and Y. Sawada, Anal. Sci., 17 (2001) 875.
11 T. Arii, T. Taguchi, A. Kishi, M. Ogawa and Y. Sawada, J. Euro. Ceram. Soc., 22 (2002) 2283.
12 T. Arii and A. Kishi, Thermochim. Acta, 400 (2003) 175.
13 T. Arii, T. Senda and N. Fujii, Thermochim. Acta, 267 (1995) 209.
14 T. Arii, Y. Sawada, N. Kieda and S. Seki, J. Mass Spectrum. Soc. Jpn., 47 (1999) 354.
15 T. Kimura, H. Imamura, M. Sugahara, T. Arii and S. Takagi, Mol. Cryst. Liq. Cryst., 176 (1996) 133.
16 S. M. Dakka, J. Therm. Anal. Cal., 74 (2003) 729.
17 T. Arii, A. Kishi and Y. Kobayashi, Thermochim. Acta, 325 (1999) 151.
18 H. Yoshida, Thermochim. Acta, 267 (1995) 239.
19 C. Allais, G. Keller, P. Lesieur, M. Ollivon and F. Artzner, J. Therm. Anal. Cal., 74 (2003) 723.
20 Entry No. 44-1087, ICDD (Indium Oxide, In_2O_3).
21 T. Arii, K. Terayama and N. Fujii, J. Thermal Anal., 47 (1996) 1649.
22 T. Arii, J. Mass Spectrom. Soc. Jpn., 51 (2003) 235.
23 A. Kishi, M. Otsuka and Y. Matsuda, Coll. Surf. B: Biointerfaces, 25 (2002) 281.